

# The global atmospheric energy transport analysed by a wavelength-based scale separation

Patrick Johannes Stoll<sup>1</sup>, Rune Grand Graversen<sup>1,2</sup>, and Gabriele Messori<sup>3,4</sup>

<sup>1</sup>Department of Physics and Technology, Arctic University of Norway, Tromsø, Norway

<sup>2</sup>Norwegian Meteorological Institute, Norway

<sup>3</sup>Dept. of Earth Sciences and Centre of Natural Hazards and Disaster Science (CNDS), Uppsala University, Uppsala, Sweden

<sup>4</sup>Dept. of Meteorology and Bolin Centre for Climate Research, Stockholm University, Stockholm, Sweden

**Correspondence:** Patrick Johannes Stoll (patrick.stoll@uit.no)

## Abstract.

The ~~global atmospheric circulation is fundamental for the local weather and climate by redistributing energy and moisture~~ atmosphere transports energy polewards in form of circulation cells and eddies. To the present day, there is a knowledge gap ~~at which spatial scales the energy and its components are transported. Therefore~~ regarding the preferred spatial scales and physical mechanisms of eddy energy transport. To investigate these, we separate the meridional atmospheric energy transport in the ERA5 reanalysis by ~~the spatial scales, the spatial scales and into~~ quasi-stationary and transient flow patterns, ~~and the latent and dry static component. We focus on the annual and seasonal mean in the transport components as well as their inter-annual variability. Motivated by similarities across latitudes in the atmospheric transport spectra when displayed as function of wavelength, we refine the existing scale separation method to~~ and latent and dry components.

Baroclinic instability is responsible for the formation of cyclones and anticyclones that vertically couple with small Rossby waves, which are considered the dominating features of the transient, synoptic scale. We find that the maxima in both baroclinically-induced and transient energy transport occur for eddies with wavelengths around 5000 km, in good agreement with the prediction by linear baroclinic theory. However, both types of transport occur within the wavelength band between 2000 and 8000 km. This result is independent of latitude. Therefore, we propose that the scale separation of the energy transport should be based on the wavelength instead of ~~wavenumber~~, the previously-used wavenumber, and use the 2000–8000 km band to define the synoptic scale. In contrast to synoptic transport, planetary transport at wavelengths around and larger than 8000 km favours situations of anomalously reduced meridional temperature contrasts.

~~This reveals advantageous, as the following conclusions can be drawn, which~~ We analyse the annual and seasonal mean in the transport components as well as their inter-annual variability. The scale-separated energy transport components are fairly similar in ~~the two~~ ~~both~~ hemispheres. Transport by synoptic waves, ~~defined at wavelengths between 2,000 and 8,000 km~~, is the largest contributor to extra-tropical energy and moisture transport, is mainly of transient character, and is little influenced by seasonality. In contrast, the transport by planetary waves, ~~larger than 8,000 km~~, highly depends on the season and has two distinct characteristics. (1) In the extra-tropical winter, planetary waves are of major importance due to ~~transport of dry static a large transport of dry~~ energy. This planetary transport ~~feature~~ features the largest inter-annual variability ~~of all components~~, and is mainly quasi-stationary in the Northern Hemisphere, but transient in its southern counterpart. (2) In the subtropical summer,

quasi-stationary planetary waves are the most important transport component mainly due to advection of moisture, which is presumably associated with monsoons. In contrast to transport by planetary and synoptic waves, only a negligible amount of energy is transported by mesoscale eddies ( $<2,000$   $<2000$  km).

## 1 Introduction

30 ~~The atmosphere is in motion~~ Atmospheric motions act to reduce the thermal contrast created by differential solar heating between high and low latitudes (Hadley, 1735). Hence the atmospheric circulation transports large amounts of energy polewards (Oort and Peixoto, 1983), and has hereby thereby a fundamental role ~~for in controlling~~ the local weather and climate (e.g. Holton and Hakim, 2013; Vallis, 2017). The energy is primarily transported in form of warm air (~~dry-stated~~ dry energy): comprising mainly of enthalpy and potential energy), and water vapour (latent energy) which releases energy when condensating 35 before precipitation (Peixoto and Oort, 1992).

The ~~manner the atmosphere is transporting energy is different among climate~~ characteristics of the energy transport differ among latitudinal zones (Trenberth and Stepaniak, 2003a). In the tropics and sub-tropics, where the Coriolis effect is small, energy is predominantly transported by a zonally-symmetric meridional overturning circulation, ~~the Hadley cell known as Hadley cell~~ (Hadley, 1735), and monsoon systems (Hadley, 1735) organised by quasi-stationary cells (Fig. 1a). In the extra-tropics, eddies ~~take over to transport the transport the majority of the~~ energy further poleward. Atmospheric eddies exist on a large range of scales, from planetary ~~and~~ Rossby waves (Rossby, 1939) and transient synoptic Rossby waves (Rossby, 1939) ~~, via that vertically interact with~~ synoptic cyclones (Bjerknes, 1919), to mesoscale disturbances, such as polar lows (Businger and Reed, 1989). Traditionally, the eddy transport is separated into a quasi-stationary and a transient component (Fig. 1a), with the former representing monthly-mean eddies and the latter ~~fast-varying faster-varying~~ deviations from this mean (Oort 40 and Peixoto, 1983). ~~Here we revise the traditional separation and compare it to a partition based on the spatial scale.~~ Transient eddies dominate the extra-tropical energy transport in both hemispheres (Fig. 1a), whereas quasi-stationary waves transport considerable amount of energy in the higher latitudes of the Northern Hemisphere (NH) and the sub-tropics of both hemispheres. They are, however, of less relevance in the extra-tropical Southern Hemisphere (SH).

Recent studies demonstrate the usefulness of separating a scale separation of the energy transport into planetary and synoptic 50 scale components, ~~as for~~. For instance, these two types of waves impact the Arctic differently (Baggett and Lee, 2015; Graversen and Burtu, 2016). The scale separation of the meridional energy transport by a zonal Fourier decomposition became popular in recent years ~~as it and~~ was applied to study the effect mechanisms and impacts of energy transport ~~for the Arctic in the Arctic region~~ (Papritz and Dunn-Sigouin, 2020; Graversen et al., 2021; Rydsaa et al., 2021; Hofsteenge et al., 2022), and ~~for the the NH~~ mid-latitudes ~~of the Northern Hemisphere (NH)~~ (Lembo et al., 2019; Röthlisberger et al., 2019; Vihma et al., 2020). 55 ~~These studies separate the transport by a wavenumber which is independent of the latitude as depicted in Figure 1b~~ (Lembo et al., 2019). ~~Further, numerous studies investigated the atmospheric dynamics in terms of Rossby waves at different spatial scales (e.g. Wirth et al., 2019)~~

~

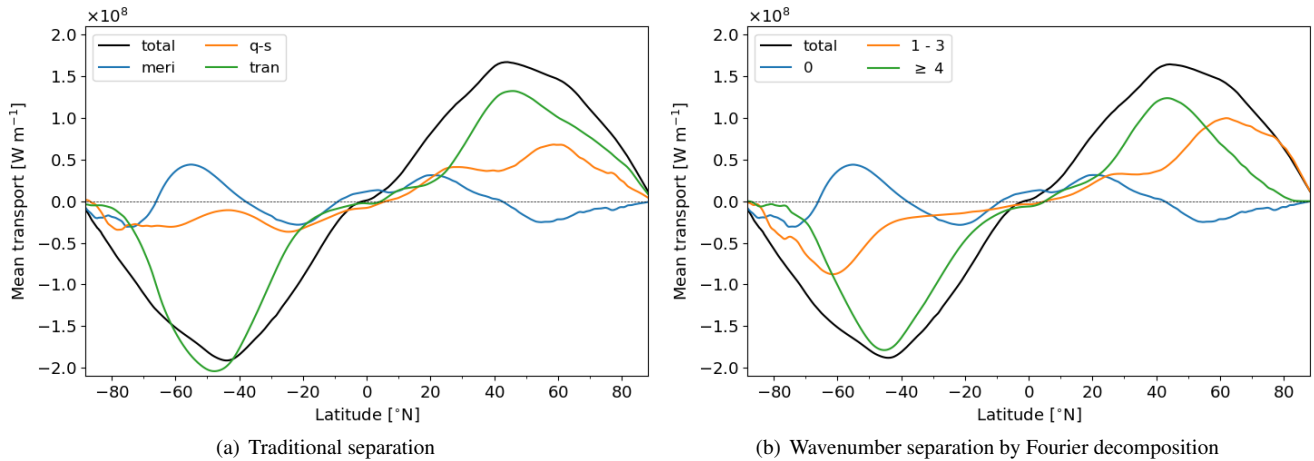


**Figure 1.** Different separation methods of the vertical-integrated, zonal-mean, northward transport of energy from ERA5 as mean of the years 1979 to 2018. (a) The traditional partition into the meridional overturning circulation (meri), quasi-stationary (q-s), and transient (tran) eddies, as performed by Oort and Peixoto (1983). (b) A decomposition into transport by different spatial scales defined by wavenumbers as suggested by Graversen and Burtu (2016). Transport by wave 0 provides the meridional overturning circulation. The sum of transport by waves 1–3 is often associated with planetary transport, whereas waves with larger wavenumbers are considered to be of synoptic scale.

Generally, the Fourier decomposition is non-local, hence the whole circle along which it is applied influences the size of the obtained eddies. This makes the Fourier decomposition useful if the circle is governed by similar eddies, which we observe from meteorological weather maps along zonal bands. Theoretically, a Fourier decomposition could be performed along longitude circles, e.g. along  $0$  and  $180^\circ$ . However, the wavelength associated with a given wavenumber is latitude-dependent (a circle going around both poles and crossing the equator twice crosses regions characterised by very different atmospheric features, making it questionable whether such a meridional Fourier decomposition provides useful insights).

However, arguably the zonal scale is connected to the meridional scale of eddies, becoming their general scale. From investigation of meteorological weather maps, we know (i) that synoptic-scale cyclones have an approximate similar zonal and meridional size since they are to first order circular, and (ii) that the meridional extent, i.e. the amplitude, of Rossby waves, appears to roughly match the distance between a trough and a ridge, featuring half a zonal wavelength. Further, we show later (e.g. Fig. 2) ~~Therefore the partitioning by wavenumber, for example between wave~~ that most of the mid-latitude transport occurs at zonal wavelengths between 2000 and 8000 ~~3 and 4 as performed in~~ km. This is in broad agreement with the finding that events of extreme transport in the mid-latitudes are largely coherent over ranges of  $10 - 30^\circ$  latitude (Lembo et al., 2019, Fig. 1d-g), considering that the event, such as a cyclone, has the size of half a zonal wavelength. Hence, as many of the previously mentioned studies ~~leads to convergence of all eddy transport to the planetary scale towards the poles, whereas synoptic transport may be overestimated at low latitudes (Fig. (Graversen and Burtu, 2016; Lembo et al., 2019, e.g.),~~ we interpret the zonal wavenumber of an eddy, which is associated with a zonal wavelength at a given latitude, as its spatial

75 scale. As previously mentioned, the typical size of the eddy is half a zonal wavelength. However, for the remainder of the study, we use the terms scale and zonal wavelength synonymously.

So far the energy transport across all latitudes has only been separated by a fixed wavenumber as shown in Figure 1b and presented by (Graversen and Burtu, 2016). Wave 3 or 4 have often been taken as the separation between planetary and synoptic scales (Baggett and Lee, 2015, e.g.). For investigation of the scale of the transport at a specific latitude or a small 80 zonal band such a separation by wavenumber is appropriate. However, the wavelength associated with a given wavenumber is latitude-dependent, which needs to be accounted for when defining the wavenumber separating spatial scales (Heiskanen et al., 2020). Wave 4 for instance corresponds to a wavelength of 8200 km at 35°, but only to 2600 km at 75°, which can be interpreted to represent different spatial scales. ~~Accordingly, Heiskanen et al. (2020) recommend to consider the threshold for separation between two wavenumbers with care~~ Such a partitioning by wavenumber thus has two caveats: i) Towards the poles all eddy 85 transport converges to the planetary scale (Fig. 1b). ii) In the subtropics, wavenumbers 1–3 appear to miss parts of planetary transport, as can be inferred from quasi-stationary eddies in the subtropical SH (Fig. 1a), being considerably larger than the planetary transport captured by wavenumbers 1–3 (Fig. 1b).

~~To circumvent this problem occurring with separation by wavenumber, we refine the scale separation method by Graversen and Burtu (2016) to be based on the wavelength instead~~ In this study, we propose a revised partition by spatial scales based on wavelength. 90 This circumvents the above-mentioned problems associated with separation by wavenumber. Hereby, we partition the transport into planetary, synoptic and mesoscale components to ~~further improve our understanding of the global atmospheric circulation~~ understand their role for transporting energy poleward. In addition, we apply the ~~established traditional~~ decomposition of the ~~energy~~ transport into stationary and transient parts (Fig. 1a), as well as ~~dry static~~ ~~dry~~ and latent components (Peixoto and Oort, 1992).

95 The new scale-separation method is employed to analyse ~~meridional energy transport by~~ the global atmospheric circulation. Previous studies found that transport by quasi-stationary waves is important in the ~~Northern Hemisphere (NH)~~ NH, but almost negligible in the ~~Southern Hemisphere (SH)~~ SH (e.g. Peixoto and Oort, 1992). Such quasi-stationary transport is often associated with the planetary scale, which appears to imply that planetary transport is irrelevant in the SH (e.g. Trenberth and Stepaniak, 2003a). In contrast, transport by transient eddies is often associated with baroclinic eddies at the synoptic scale (e.g. 100 Trenberth and Stepaniak, 2003a). However, transport at other scales could be of transient character as well. In this study, we ~~are pointing out~~ ~~underline~~ that the separation of transport into a quasi-stationary and transient contribution is different from a separation into planetary and synoptic scales. ~~Although, although~~ a correlation exists between the two, especially for the NH.

To summarise the main research questions posed in this study:

1. ~~At what scales does the atmosphere transport energy?~~
2. ~~How does the traditional separation method compares to the scale separation method~~ ~~What useful information do the different partitions of the atmospheric energy transport provide?~~
3. ~~What characterises the atmospheric energy transport in different climate zones~~ ~~meridional bands?~~

These questions are targeted in Sections 3 and 4. The main results are then summarised and discussed in Section 5. However, first we present the utilised data and methods are presented.

## 110 2 Data and methods

### 2.1 ERA5 reanalysis

The atmospheric energy transport from for the period 1979 – 2021 is analysed with ERA5 (Hersbach et al., 2020), the fifth atmospheric reanalysis from the European Centre for Medium-Range Weather Forecasts (ECMWF), which substituted its precursor ERA-I in 2019. ERA5 provides hourly fields at a spectral truncation of T639, which is equivalent to a grid spacing 115 of 30 km with 137 vertical hybrid levels. For this study, fields of temperature, air temperature, specific humidity, geopotential height and horizontal wind components at all hybrid levels, and surface pressure and surface topography are used at on a  $0.25^\circ \times 0.25^\circ$  horizontal grid spacing. Since reanalysis data are prone to include mass-flux inconsistencies (Trenberth, 1991), a barotropic mass-flux correction is applied to the wind field prior to calculating the energy transport (Graversen, 2006).

In this study, we take a zonal-mean perspective of the atmospheric energy transport, which provides the transport through 120 an atmospheric column with one metre width. Hereby, it provides a local measure of the transport, and differs from other studies that zonally integrate the transport along each longitude circle (Peixoto and Oort, 1992; Trenberth and Caron, 2001; Graversen and Burtu, 2016). However, the computed

### 2.2 Zonal mean versus zonal integral

The zonal integral of the energy transport from ERA5 (Fig. S1a) confirms the transport in these studies found in previous studies 125 using data sets with lower spatial resolution (Peixoto and Oort, 1992; Trenberth and Caron, 2001; Graversen and Burtu, 2016). For instance, the zonal-integrated poleward transport peaks at  $4.8 \times 10^{15}$  W in the NH and  $5.6 \times 10^{15}$  W in the SH at  $41^\circ$  latitude in both hemispheres. The latitude of maximum zonal-mean transport is slightly higher at  $45^\circ$ . By computing the zonal integral of the energy transport, which depends on the length of the longitude circle, the transport becomes small at high latitudes since the longitudes converge (Fig. S1b). Further, the average transport. However, the local transport, expressed by the zonal mean, is 130 considerable also in the polar regions is more easily assessed by the zonal-mean transport as it is not influenced by converging latitudes.

The (Fig. S1b). Hence, to compare the local importance of the atmospheric energy transport across all latitudes, we take a zonal-mean energy transport is smoothed with a  $2^\circ$  perspective which provides the transport through an atmospheric column with one metre width. The latitude of maximum zonal-mean transport, namely the location at which the largest local meridional 135 transport occurs, is at  $45^\circ$  latitude in both hemispheres (Fig. running-mean filter along the meridional dimension for noise reduction. S1b), different to the maximum zonally-integrated transport peaking at  $41^\circ$ .

For the calculation of convergence of energy transport this, a  $2^\circ$  running-mean filter is used before and after along the meridional dimension before computing the meridional derivatives.

## 2.3 Decomposition of the energy transport

140 The atmospheric energy transport and its components are characterised by a large day-to-day variability (Lembo et al., 2019) (Swanson and Pierrehumbert, 1997; Messori and Czaja, 2013; Swanson and Pierrehumbert, 1997). However, we take a here we focus on the annual-mean and season-mean perspective of the energy transport, since one purpose of this study is the comparison of firstly to investigate the "normal" circulation, and secondly to compare the traditional separation of the transport by quasi-stationary and transient eddies with a separation based on spatial scales. This comparison is only possible from a 145 time-mean perspective, since the computation of quasi-stationary transport is normally derived based on monthly-mean fields (Oort and Peixoto, 1983). A eddy transport requires a predefined time period over which the eddies are considered stationary, which is traditionally set to one month (Oort and Peixoto, 1983). Since this study focuses on the mean transport, a subsequent study is planned for investigating the short time variability short-time variability and the extremes of the different energy transport components.

150 This study investigates the vertically-integrated, zonal-mean, time-mean, meridional transport of atmospheric energy,

$$\widetilde{vE} = \int_0^{p_s} [\overline{vE}] \frac{dp}{g}, \quad (1)$$

where  $\mathbf{v} = (u, v)$  are the zonal and meridional wind components,  $v$  is the meridional wind,  $E$  an energy component is the atmospheric energy,  $p$  pressure,  $p_s$  surface pressure,  $g$  the gravitational constant,  $\overline{\cdot}$  denoting denotes a monthly time average, and  $[\cdot]$  the zonal average. We decompose the total atmospheric energy transport,  $\widetilde{vE}$ , in three ways that can be applied in combination succession:

155 1) Into The total atmospheric energy transport,  $\widetilde{vE}$ , is partitioned into latent energy transport,  $\widetilde{vQ}$ , and dry-static-energy transport dry energy transport,  $\widetilde{vD}$ , following (Oort and Peixoto, 1983). This is archived achieved by separating the energy total atmospheric energy,  $E$ , in Equation 1 into its latent component,  $Q$ , and dry-static dry component,  $D$ , comprising which comprises the enthalpy,  $C_p T$ , potential energy,  $gz$ , and kinetic energy,  $\frac{\mathbf{v}^2}{2}$ ,

$$E = Q + D = Lq + \left( C_p T + gz + \frac{\mathbf{v}^2}{2} \right), \quad (2)$$

160 with  $q$  being specific humidity,  $L$  the latent heat release by condensation,  $C_p$  specific heat capacity at constant pressure, and  $T$  temperature, and  $\mathbf{v}$  the horizontal wind vector.

2) Into monthly-mean The total energy transport,  $\widetilde{vE}$ , expressing an time-mean transport, is separated into transport by transient eddies,  $\widetilde{vE}^{tran} - \widetilde{vE}^{tran} = \int_0^{p_s} [\overline{v'E'}] \frac{dp}{g}$ , quasi-stationary eddies,  $\widetilde{vE}^{q-s} - \widetilde{vE}^{q-s} = \int_0^{p_s} [\overline{v^*E^*}] \frac{dp}{g}$ , and the mean meridional circulation,  $\widetilde{vE}^{meri}$ , derived by the following equation according to Peixoto and Oort (1992)  $\widetilde{vE}^{meri} = \int_0^{p_s} [\overline{v}][\overline{E}] \frac{dp}{g}$ , by 165 partitioning the zonal-mean, time-mean transport,  $[\overline{vE}]$ , in Equation 1 according to Oort and Peixoto (1983) and Peixoto and Oort (1992) by

$$[\overline{vE}] = [\overline{v'E'}] + [\overline{vE}] = [\overline{v'E'}] \pm [\overline{v^*E^*}] + [\overline{v}][\overline{E}], \quad (3)$$

with  $\cdot'$  denoting anomalies from the time mean, and  $\cdot^*$  stating denoting zonal anomalies from the zonal mean. The first equality is separating the time-mean transport into the transport by the time-mean fields,  $[\overline{vE}]$ , and by faster-varying fluctuations,  $[\overline{v'E'}]$ .

170 The second equality partitions the former term into a zonally-symmetric transport,  $\langle \tilde{v} \rangle \langle \tilde{E} \rangle$ , and a contribution by zonal waves,  $\langle \tilde{v}^* \tilde{E}^* \rangle$ . In principle the duration of the time mean,  $\langle \cdot \rangle$ , for which eddies are considered quasi-stationary is arbitrary. However, traditionally the mean is taken over one month periods (Oort and Peixoto, 1983). Hereby, the quasi-stationary transport eddy transport,  $\langle \tilde{v}^* \tilde{E}^* \rangle$ , provides the transport given by the monthly-mean fields eddies, and the transient transport,  $\langle \tilde{v} \tilde{E} \rangle$ , is the residual fast varying component. The annual-mean energy transport partitioned in this traditional manner is depicted in  
175 Figure 1a. The transport of latent energy,  $\tilde{v} \tilde{Q}$ , and dry energy,  $\tilde{v} \tilde{D}$ , is partitioned in a similar manner.

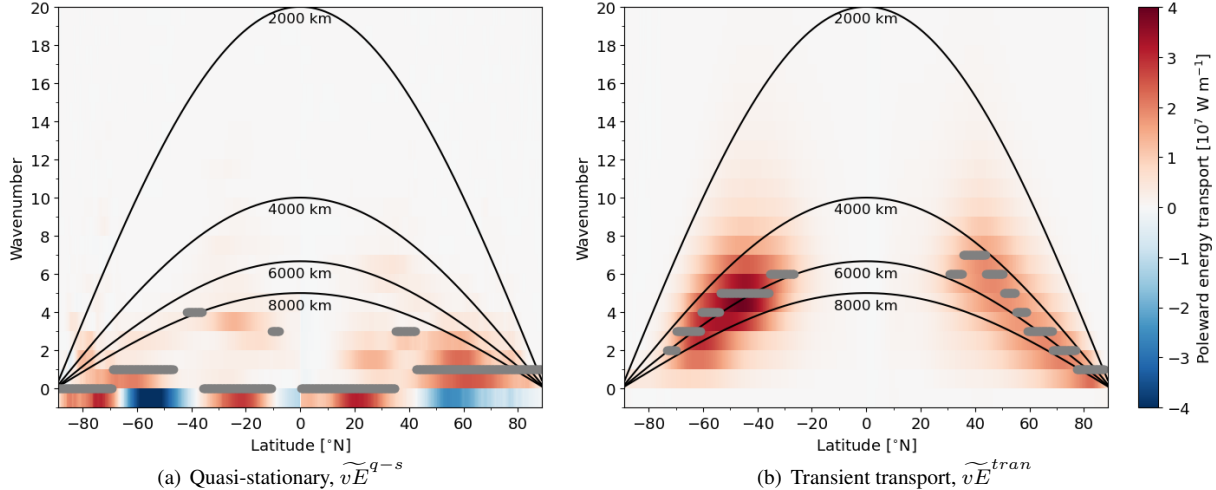


Figure 2. The annual-mean, zonal-mean of the Fourier-decomposed poleward transport of energy from ERA5 for by each latitude wave at all latitudes. (a) Depicts the decomposition of the quasi-stationary and (b) of the transient energy transport. The wavenumbers corresponding to some wavelengths of 2000, 4000, 6000 and 8000 km are presented depicted by black curves. The solid curves at 2,000 km and 8,000 km denote last curve separate the transport into the separation between meso, synoptic and planetary scale. At each latitude the wave of maximal poleward energy transport is denoted in grey, where values are masked if the wave is responsible for less than 5% of the transport at the latitude with maximum transport.

3) Into planetary-scale transport,  $\tilde{v} \tilde{E}_{plan}$ , synoptic-scale transport The total energy transport,  $\tilde{v} \tilde{E}$ , is lastly separated into transport by eddies at the planetary scale,  $\tilde{v} \tilde{E}_{plan}$ , the synoptic scale,  $\tilde{v} \tilde{E}_{syno}$ , mesoscale transport and the mesoscale,  $\tilde{v} \tilde{E}_{meso}$ , and as well as the meridional circulation,  $\tilde{v} \tilde{E}_{meri}$ . For the partition into spatial scales the Fourier decomposition is applied along each latitude,  $\phi$ , and at each vertical model level, and at every time step for  $E$  and  $v$  following Graversen and Burtu  
180 (2016),

$$E = \frac{a_0^E}{2} \frac{a_0^E}{2} + \sum_{n=1}^{\infty} a_n^E \cos \left( \frac{n2\pi x}{d} \right) + b_n^E \sin \left( \frac{n2\pi x}{d} \right), \quad (4)$$

with  $x$  the zonal coordinate,  $d = 2\pi a \cos(\phi)$ ,  $a = 6371$  km Earth's radius, and the coefficients:

$$a_n^E = \frac{2}{d} \oint E \cos \left( \frac{n2\pi x}{d} \right) dx, \quad b_n^E = \frac{2}{d} \oint E \sin \left( \frac{n2\pi x}{d} \right) dx. \quad (5)$$

In a similar manner coefficients are derived. The coefficients for the meridional wind,  $v$ :  $a_n^v$  and  $b_n^v$ , are derived in a similar manner.

185

The transport associated with the meridional circulation is then given by:

$$[vE]_{meri} = \frac{1}{4} a_0^v a_0 \underbrace{E}_{\sim}. \quad (6)$$

which becomes similar to  $\widetilde{vE}^{meri}$  for monthly time averages.

The zonal-mean transport by wave  $n$  is becoming given by

$$190 \quad [vE]_n = \frac{1}{2} \left( a_n^v a_n \underbrace{E}_{\sim} + b_n^v b_n \underbrace{E}_{\sim} \right). \quad (7)$$

The Note, that the cross terms  $a_n^v$  and  $a_m^E$  with  $n \neq m$ , and similarly  $b_n^v$  and  $b_m^E$ , vanish since the Fourier components feature an orthogonal basis.

195

This partition is applied to the instantaneous co-variability,  $vE$  in Equation 1, resulting in the wave-separated total transport, as well as to the transport by monthly-mean fields,  $\bar{vE}$  in Equation ??, resulting in the wave-separated quasi-stationary transport,  $\widetilde{vE}^{q-s}$ . The annual-mean transport by each wave as quasi-stationary wave (applying Eq. 7 on  $[\bar{vE}]_n$ ) as a function of latitude is displayed in Figure 2 for the quasi-stationary and transient transport components. The wave-separated transient transport,  $\widetilde{vE}^{tran}$ , (Fig. 2b) is derived by subtracting the quasi-stationary component from the total wave-separated transport given by Equation 7.

195

To separate the energy transport between the scale  $s$  and the next smaller scale  $s+1$  (at larger wavenumber) based on the predefined wavelength,  $\lambda_{s+1}$ , the latitudinal-dependent ( $\phi$ ) separation (wave) number,  $n_{s+1}$ , is computed based on the predefined wavelength,  $\lambda_{s+1}$ :

$$n_{s+1} = \frac{2\pi \cdot a \cdot \cos(\phi)}{\lambda_{s+1}}. \quad (8)$$

To separate planetary waves from the meridional overturning circulation,  $n_{plan} = 0$  is applied. For the separation between planetary and synoptic waves, the separation number,  $n_{syno}$ , is computed at each latitude from the wavelength  $\lambda_{syno} = 8,000 \lambda_{syno} = 8000$  km (lower black solid line in Fig. 2). Synoptic and mesoscale eddies are separated at a wavelength of  $\lambda_{meso} = 2,000 \lambda_{meso} = 2000$  km.

205 In Section 3, we argue for the usage of these two wavelengths for scale-separating the energy transport. The separation numbers as defined here are real numbers. To ensure a continuous separation (Fig. S2ab), instead of abrupt transitions (Fig. S2ba), the transport given by eddies of spatial scale,  $s$ , is defined by:

$$[vE]_s = ([n_s] - n_s) \cdot [vE]_{[n_s]} + \sum_{n=[n_s]+1}^{\lfloor n_{s+1} \rfloor} [vE]_n + (n_{s+1} - \lfloor n_{s+1} \rfloor) \cdot [vE]_{\lceil n_{s+1} \rceil}, \quad (9)$$

210 with  $\lfloor \cdot \rfloor$  rounds denoting rounding to the integer part and  $\lceil \cdot \rceil$  rounds rounding to the least integer. Equation 9 provides the This provides the latitude-dependent separation depicted in Figure 2 between the black solid lines representing the separation numbers. curves at 2000 and 8000 km.

An underlying interpretation is that at a latitude circle of for instance 30,000 longitude circle with for example 20000 km extent (at 60° latitude), wave 1 includes the energy transport at a scale larger than 15,000 of and larger than the longitude

215 cycle, wave 2 between 10000 and 20000 km, and so forth. Hereby, wave 2 of between this and 10,000 with a wavelength of 6700 km provides the transport between its wavelength and 10000 km and so forth is accordingly equally partitioned between the synoptic and planetary scale since the separation number for the synoptic scale is  $n_s = 2.5$  meaning that  $[n_s] - n_s = 0.5$  of eddy  $[n_s] = 3$  (first term in Eq. 9) is associated with the synoptic scale.

220 This continuous partition of the transport by the first wave smaller than 8000 km, leads to the synoptic scale including less transport than the application of a strict separation (Fig. S2). Hence, waves at wavelength around and larger than 8000 km are associated to the planetary scale, whereas the synoptic scale constitutes waves strictly smaller than 8000 km. Spectra depicting the separation into the scale components at different latitudes are provided in Figure S3 and an example for a detailed illustration of the separation is provided in Supplement Section 3. It should be noted that Wolf and Wirth (2017) applied a related continuous scale separation for the latitude-dependent detection of Rossby wave packages. The same procedure of 225 scale separation is applied to the latent and dry energy transport.

### 3 Wavelengths utilised for scale separation

Orlanski (1975) defines the mesoscale to be smaller than 2,000 km, which is commonly accepted and hence utilised as threshold in this study for separation towards the larger as lower threshold for the synoptic scale. However, a widely-agreed separation between the planetary and synoptic scale scales has not been established. For the following reasons we implement 230 Below, we argue for placing the separation between the planetary and synoptic scale scales at a wavelength of 8,000 km, even though the exact value is to some degree arbitrary. As previously presented this partition is done in a continuous manner, such that transport at and around the wavelength of 8000 km is associated to the planetary scale, whereas synoptic waves are considered to be strictly smaller than this threshold.

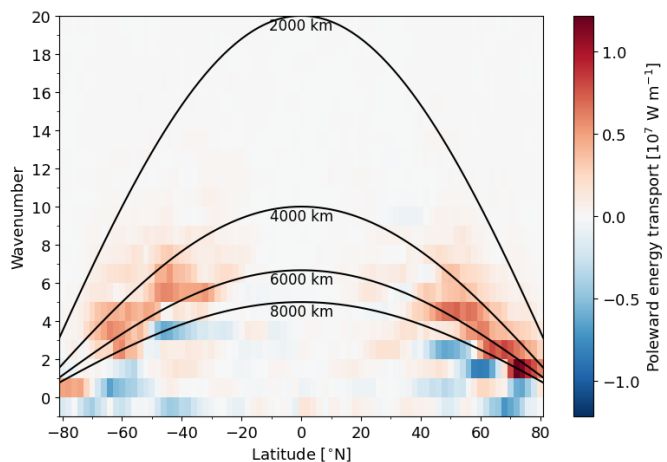
④

#### 235 3.1 Theoretical baroclinic argument

Baroclinic instability is recognised as the single dominant instability of the synoptic scale (Markowski and Richardson, 2011, p.4). The synoptic scale is thus supposed to include most energy transport associated with synoptic cyclones transports associated 240 with eddies developing by baroclinic instability (Vallis, 2017; Holton and Hakim, 2013). The Synoptic eddies are typically identified as cyclones and anticyclones in sea-level pressure. They interact vertically and baroclinically with upper-tropospheric oscillations of the jet stream, often referred to as transient synoptic Rossby waves (e.g. Röthlisberger et al., 2019; Ali et al., 2021). The theoretical scale (wavelength) of baroclinic eddies is given by 3.9 times the Rossby deformation radius,  $L_d$ , and hence estimated to be 4,000 km by (Vallis, 2017, p.354) and 4,800 km by Stoll et al. (2021) using more exact values obtained 245 from extra-tropical cyclones. Note, that a low pressure low (high) pressure system spans half a wavelength, and has accordingly a typical size of around 2,000 diameter of around 2000 km. Since synoptic cyclones feature some variability in their size, and in the Fourier decomposition considerable amount of the energy transport is occurring on neighbouring waves (Heiskanen et al., 2020, Fig. 3), a

250 ~~A wavelength band between 2,000–8,000 km appears appropriate to capture the majority of the transport associated with synoptic eyelines. However, this band also includes transient synoptic Rossby waves (e.g. Röthlisberger et al., 2019; Ali et al., 2020, which may interact with eyelines in a baroclinic manner. Also other processes than baroclinic instability, likely contribute to the formation of baroclinically-induced synoptic eddies for two reasons: (i) Synoptic eddies, such as cyclones and anticyclones, feature some variability in their size, but with a typical diameter between 1000 and smaller than 4000 km. (ii) The non-local Fourier decomposition of the energy transport in situations of localised synoptic cyclones captures considerable transport at neighbouring waves to the cyclone (Heiskanen et al., 2020, Fig. 3), which may be considered a weakness of the Fourier decomposition. However, the here-defined synoptic eddies, such as heating contrasts. A future study is going to investigate the causes for eddy transport at different scales. band of wavenumbers around the localised eddy appears to be appropriate to capture the eddy.~~

255 ~~2) Previous studies performing a wave decomposition qualitatively agree on the separation at a wavelength of 8,000~~



260 **Figure 3.** The composite of the anomalous poleward energy transport by individual waves ( $[vE]_n$  of Eq. 7) at different latitudes 4 days after situations of anomalous high (90 percentile) meridional temperature contrasts around the latitude of energy transport. The anomalies on a daily resolution are computed from the 21 day and 9 year running mean climatology. The meridional temperature contrast is computed by the difference between the zone  $10^\circ$  equatorward and  $10^\circ$  poleward of the latitude of interest. Hence, red colours denote waves transporting more energy polewards 4 days after situations of enhanced meridional temperature differences. The wavenumbers corresponding to wavelengths of 2000, 4000, 6000 and 8000 km are depicted by black lines. Wave 0, is corrected by the meridional mass flux to express the instantaneous zonal mean transport according to Lembo et al. (2019).

### 3.2 Statistical baroclinic argument

265 ~~Figure km:2a) Baggett and Lee (2015) perform a Fourier decomposition of energy characteristics for the entire NH and demonstrate different life-cycle behaviour of long (planetary) and short (synoptic) waves for a separation between wave 3 and 4. Ali et al. (2021) identifies recurrent synoptic-scale transient Rossby wave packets in the mid-latitudes at wavenumbers between 3 depicts the~~

anomalous daily energy transport by different waves for situations 4 days after enhanced meridional temperature gradients (90 percentile). Different time differences provide similar results (not shown) and 15. Their separation into planetary and synoptic eddies between waves 3 and the presented one of 4 is similar to the here applied partitioning at a wavelength of 265 8,000 days is in good agreement with Figure 1a of Baggett and Lee (2015). The separation between waves featuring enhanced and decreased transport as response to the increased thermal contrast is at around 8000 km at 53° latitude which is close to the zone of maximum eddy activity (Fig. 2 for all latitudes in the extra-tropics. Waves whose energy transport is most closely associated with the increased temperature gradient have a wavelength between 3000 and 8000 km). For a hemisphere-wide separation into planetary and synoptic eddies with one wavenumber of separation as utilised by Baggett and Lee (2015) and 270 Ali et al. (2021), it appears crucial to capture the partition around this zone.

2b) At 70 km with a maximum transport anomaly for wavelengths around 5000 N, a wavelength of 8,000 km is associated with a separation number  $n_{syno} = 1.7$ , meaning that 70% of wave 6000 is associated with the planetary scale and 30% to the synoptic scale. Accordingly, the lead-lag regression of the Arctic temperature to the latent transport presented in km. Since 275 baroclinic instability is induced by a horizontal temperature gradient, this provides a strong statistical evidence, in agreement with the theoretical argument from the previous section, that baroclinic instability is an important development mechanism for the synoptic waves as defined in this study. In the following, we refer to the anomalous energy transport 4 days after situations of enhanced meridional temperature gradients as "baroclinically-induced transport anomaly". The strength of the baroclinically-induced transport anomaly by the synoptic waves (Fig. 6 of Graversen and Burtu (2016) shows a clear difference 280 between wave 1, leading to heating of the Arctic, and waves 3 and larger, having a baroclinic signal. Wave 2 appears to share characteristics between the wave 1 and waves larger than 2, in agreement with the here applied separation number that divides wave 3 at wavelength between 2000 and 8000 km. Also Heiskanen et al. (2020) find a good attribution of an idealised cyclone to the synoptic scale, if the separation between the planetary and synoptic scale is performed at rather small wavenumbers 285 even though they do not test a separation between wave km) is around a third of the time-mean energy transport of these waves (Fig. 2 and 3, 2), so it is considerable. The mean meridional temperature contrast will also induce baroclinic waves transporting energy, which is not captured by this methodology.

3) The latitudinal independence of the wavelength of the baroclinically-induced transport anomaly provides a major argument for using a wavelength threshold to separate between the synoptic and planetary scales rather than a wavenumber threshold. It is surprising that the scale of maximum baroclinically-induced transport anomaly is independent of the latitude, 290 since the Rossby deformation radius,  $L_d = \frac{NH}{f}$ , estimating the size of baroclinic eddies (Vallis, 2017), depends inversely on the Coriolis parameter,  $f$ , increasing with latitude, and depends linearly on the depth of the troposphere,  $H$ , and the tropospheric static stability,  $N$ , which could be argued to rather decrease with latitude (Stoll et al., 2021). Hence, baroclinic eddies would be expected to be smaller at higher latitudes. A hypothesis for the latitude-independence of the baroclinic eddies is as follows. Most extra-tropical cyclones originate from the mid-latitudes, where the meridional temperature contrast is largest. The size of a cyclone is set during the genesis stage when the fastest-growing mode is prevailing. Many cyclones propagate to higher 295 latitudes along the diagonal axis of the storm tracks (Shaw et al., 2016) and may preserve their original size.

We note that processes other than baroclinic instability may contribute to the formation of the here-defined synoptic eddies, such as heating contrasts. A future study is going to further investigate the drivers of eddy transport at different scales.

### 3.3 Transient and quasi-stationary eddies

In the following we show that the partition at a wavelength of ~~8,000~~<sup>8000</sup> km approximately captures our intuitive understanding that synoptic cyclones and synoptic Rossby wave packets are transient by nature, whereas planetary waves are more quasi-stationary, since they may be constraint by ~~locally-fixed~~ orography and large-scale ~~and~~ semi-stationary thermal forcing, such as heating contrasts between ocean and land (Vallis, 2017),~~as we show in the following:~~

The spectral decomposition of the annual-mean energy transport,  $\widetilde{vE}$ , at different latitudes reveals that most eddies smaller than ~~8,000~~<sup>8000</sup> km are of transient nature, whereas most of the quasi-stationary transport is at scales larger than ~~8,000~~<sup>8000</sup> km (Fig. 2). This is in good agreement with Dell'Aquila et al. (2005) who found in the average of the extra-tropical NH, that wave 3 features a typical time period of around a month whereas smaller eddies, here associated to the synoptic scale, are characterised by weekly or daily periods.

For the transient energy transport, the wavenumber of maximum transport is 6 or 7 in the subtropics and decreases towards the poles, such that the corresponding wavelength of maximum transient transport is around ~~5,000 to 6,000~~<sup>5000 to 6000</sup> km for all latitudes. Also in the moisture transport, the transient component reaches its maximum around 5000 km (Fig. S4), which is in good agreement with Lee et al. (2019). This wavelength corresponds well to the preferred scale of baroclinic eddies (~~4,000–5,000 km~~ Vallis, 2017; Stoll et al., 2021). The (~~4000–5000 km~~: Vallis, 2017; Stoll et al., 2021), and of baroclinically-induced transport anomalies presented in the previous section. The latitudinal independence of the ~~scale wavelength~~ of maximum transient transport ~~from latitudes~~ provides a major argument that the separation between the synoptic and planetary scale is better achieved by a threshold based on wavelength rather than wavenumber when the transport across all latitudes is examined.

It may appear surprising that the scale of maximum transient energy transport,  $\widetilde{vE}^{tran}$ , is independent of the latitudes, since the deformation radius estimating the size of baroclinic eddies depends inversely on the Coriolis parameter, and depends linearly on the layer depth which decreases with latitude (Vallis, 2017). However, these are parameters important for the cyclogenesis which is mostly active in a confined region. Most cyclones originate from the mid-latitudes, where the horizontal temperature contrast is largest. The size of a cyclone is set during the genesis stage when the fastest-growing mode is prevailing. Many cyclones propagate to higher latitudes along the diagonal axis of the storm tracks (Shaw et al., 2016) and may keep their size~~supports~~ separating the planetary and synoptic scale by the use of wavelength instead of wavenumber.

The preferred wavenumber and wavelength of the quasi-stationary transport,  $\widetilde{vE}^{q-s}$ , are latitude dependent (Fig. 2a). The wavenumber of maximum quasi-stationary transport is larger than ~~8,000~~<sup>8000</sup> km everywhere besides close to the North Pole where the Fourier decomposition is not applicable and around 40° S where the quasi-stationary transport is almost negligible. A short analysis of the preferred scales of the quasi-stationary transport is provided in Supplement [Section 4](#).

Based on the partitioning into transient and quasi-stationary eddies, we here argue for the wavelength of ~~8,000~~<sup>8000</sup> km for separating between synoptic and planetary waves. However, it is evident that the traditional decomposition of the transport

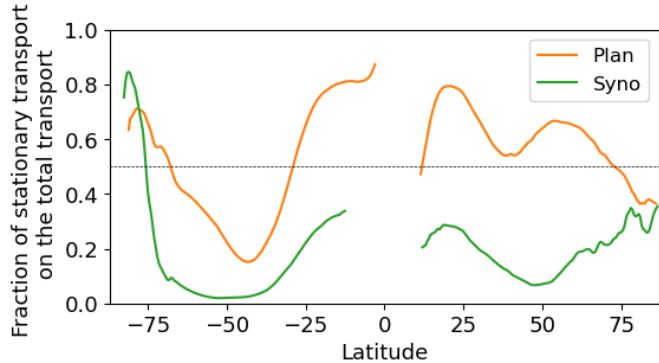


**Figure 4.** The fraction of the quasi-stationary part of the transport by planetary and synoptic waves as a function of latitude ~~from~~<sup>in</sup> ERA5.

330 into stationary and transient parts (Oort and Peixóto, 1983) is not equivalent to a separation into planetary and synoptic waves: Planetary waves at a wavelength larger than ~~8,000~~<sup>8000</sup> km can be both transient and quasi-stationary (Fig. 2). In the latitude band between 70 and 30° S and poleward of 70° N, zones mainly characterised by open ocean, the transient component within the planetary transport is larger than the quasi-stationary component (Fig. 4). At latitudes with more land, the quasi-stationary component is responsible for ~~50~~<sup>50</sup>–80% of the planetary transport, meaning that also at these latitudes a considerable proportion 335 of the planetary transport is transient. Also the moisture transport,  $\tilde{v}Q$ , comprises a planetary component that features ~~both~~<sup>both</sup> transient and quasi-stationary ~~characteristics~~<sup>contributions</sup>, similar to the total energy transport  $\tilde{v}E$  (Fig. S5).

In contrast ~~to planetary transport~~, the synoptic transport is mainly ~~(70–100%)~~ of transient nature at ~~almost~~ all latitudes, which coincides with the transient character of synoptic cyclones and Rossby waves of short ~~wave length~~. ~~Hence in the following,~~ wavelength. The small quasi-stationary contribution (0–30%) to the synoptic transport is attributed to preferred 340 spatial locations for synoptic activity. For instance, the NH Atlantic sector features more cyclonic activity than other longitudes, which in the time-mean results in increased quasi-stationary transport. This can be inferred from Rydsaa et al. (2021), who show a large time-mean synoptic transport in the Atlantic sector for strong latent transport events in winter at 70° N. However, in a zonal-mean perspective the quasi-stationary ~~component of~~ contribution to the synoptic transport is small (< 30%) compared 345 to its transient part. Hence, for the sake of simplicity the synoptic transport is not ~~further investigated~~, separated into a transient and quasi-stationary contribution in the remainder of this study.

An exception for the transient character of synoptic transport is over Antarctica, which is characterised by katabatic flows advecting cold air towards lower latitudes, occurring at preferred locations of drainage, hence including a large stationary component.

~~In conclusion, a separation at 8,000~~

350 **3.4 Comparison to previous studies**

Previous studies performing a wave decomposition qualitatively agree on the separation at a wavelength of 8000 km:

1) Baggett and Lee (2015) perform a Fourier decomposition of energy characteristics for the entire NH and demonstrate different life cycle behaviour of long (planetary) and short (synoptic) waves for a separation between wave 3 and 4. Ali et al. (2021) identify recurrent synoptic-scale transient Rossby wave packets in the mid-latitudes at wavenumbers between 4 and 15.

355 Wirth et al. (2018) note that planetary- scale Rossby waves are typically characterised by zonal wavenumbers 1–3, whereas synoptic-scale Rossby waves are characterised by higher wavenumbers.

Their separation into planetary and synoptic eddies between waves 3 and 4 is similar to the here-applied partitioning at a wavelength of 8000 km ~~appears to capture our intuitive understanding of~~ at  $53^{\circ}$  latitude which is close to the location of maximum eddy activity (Fig. 1). For a hemisphere-wide separation into planetary and synoptic eddies with a single wavenumber 360 threshold as utilised by Baggett and Lee (2015) and Ali et al. (2021), it appears crucial to capture the partition around this latitude.

2) At  $70^{\circ}$  N, a wavelength of 8000 km is associated with a separation number  $n_{syno} = 1.7$ , meaning that 70% of wave 2 is associated with the planetary scale and 30% to the synoptic scale. Accordingly, the lead-lag regression of the Arctic temperature on the latent transport presented in Fig. 6 of Graversen and Burtu (2016) shows a clear difference between wave 1, leading to 365 heating of the Arctic, and waves 3 and larger, having a baroclinic signal. Wave 2 appears to share characteristics of both wave groups, in agreement with the here-applied partition of wave 2 at  $70^{\circ}$  N. Also Heiskanen et al. (2020) find a good attribution of the meridional energy transport by an idealised cyclone to the synoptic scale, if the separation between the planetary and synoptic scales is performed at rather small wavenumbers, even though they do not test a separation between wave 2 and 3.

In conclusion, a separation at wavelengths of 8000 km is consistent with previous interpretations of planetary and synoptic 370 scale transports. However, as mentioned earlier, a ~~clear~~ sharp threshold likely does not exist. Therefore, the separation wavelength of ~~8,000~~ 8000 km is compared to wavelengths of ~~10,000~~ 10000 km and ~~6,000~~ 6000 km in the Supplement (Fig. S6). The main results of this study are not affected by the exact choice of the separation wavelength, as shortly discussed in the Supplement.

## 4 Organisation of the global energy transport

375 In this section, we analyse the atmospheric energy transport from ERA5 by utilising the scale-separation method. The applied ~~climate zones~~ ~~latitudinal bands~~ used in this study are provided in Table 1.

### 4.1 Annual-mean transport

#### Overview

The meridional atmospheric energy transport features large similarities ~~for in~~ the two hemispheres in most components and 380 for most climate zones (Fig. S6) ~~and~~. Hence, to simplify the comparison of the two hemispheres, we display the poleward transport of both hemispheres at different latitudes on a common ~~axis~~ x-axis (Fig. 5a–c).

**Table 1.** The applied ~~climate zones~~ terms to describe latitudinal bands in this study.

Climate zone	Latitude band
Equatorial region	< 10°
Tropics	< 23°
Sub-tropics	23° <del>–</del> <sup>~</sup> 35°
Extra-tropics	35° <del>–</del> <sup>~</sup> 90°
Mid-latitudes	35° <del>–</del> <sup>~</sup> 60°
Polar boundary	Around 60°
Polar regions	60° <del>–</del> <sup>~</sup> 90°

The annual-mean, zonal-mean poleward energy transport,  $\widetilde{vE}$ , is seamless in the sense that it resembles half of a sine curve for both hemispheres (black lines in Fig. 5a) as noted by Trenberth and Stepaniak (2003b). ~~The poleward atmospheric energy transport is almost similar in both hemispheres~~ ~~In the SH subtropics and mid-latitudes~~, however, ~~it is  $\approx$  15% larger in the subtropics and mid-latitudes of the SH than than in the~~ the NH, ~~largely which is~~ balanced by more oceanic transport in the NH (Trenberth and Caron, 2001).

The energy transport,  $\widetilde{vE}$ , ~~causes leads to an~~ annual-mean divergence of around  $40 \text{ W m}^{-2}$  in the tropics and subtropics and convergence ~~at latitudes~~ poleward of  $40^\circ$  latitude of up to  $100 \text{ W m}^{-2}$  in the polar regions (Fig. 5d) in good agreement with Trenberth and Stepaniak (2003a). The smaller divergence close to the equator is due to oceanic currents transporting heat to the subtropics and hence creating a cold tongue of sea-surface temperatures over the equatorial Pacific (Trenberth and Stepaniak, 2003b).

Despite the total energy transport,  $\widetilde{vE}$ , appearing seamless, different transport mechanisms are important in the ~~climate zones expressed different climate zones, as reflected~~ by a considerable variations across latitudes in the moisture and ~~dry static~~ ~~transport dry transports~~ (Fig. 5b and c), and in the scale components of the transport.

~~To a first order, the~~ ~~The total~~ annual-mean moisture transport,  $\widetilde{vQ}$ , ~~resembles the inverse of a sine curve in each hemisphere with an exponentially decaying tail towards the poles of both hemispheres features equatorward extremes at around 10°~~ (Fig. 5b). ~~Hence, moisture transport in the tropics is equatorward and poleward in the subtropics and extra-tropics with a maximum poleward maxima at~~ around  $40^\circ$  ~~latitude~~ and decaying tails towards the poles. This leads to moisture divergence in the non-equatorial tropics and sub-tropics ~~and convergence, whereas moisture converges~~ in the equatorial regions and extra-tropics (Fig. 5e). ~~The dry static~~ ~~The moisture transport is generally stronger in the Southern than Northern Hemisphere, due to more evaporation on the water surfaces of the SH. Further, some moisture is transported across the equator from the SH to the NH leading to the highest convergence of moisture at around 7° N, which is in the annual mean the approximate location of the intertropical convergence zone (ITCZ).~~

405 The dry transport,  $\widetilde{vD}$ , features a plateau between 10–65° latitude (Fig. 5c) and decays towards the equator and poles. Hence, it is mainly responsible for divergence in the equatorial regions and convergence in the polar regions (Fig. 5f). However, the scale components have different roles in the different climate zones.

### Synoptic transport

Synoptic-scale waves are dominant in the transport of energy in the mid-latitudes of both hemispheres (Fig. 5a). Although synoptic transport is around 40% stronger in the SH than the NH. This is in broad agreement with the finding of Peixoto and Oort (1992) that transient transport is more relevant in the SH, but keeping in mind that some of the transient transport occurs at the planetary scale (Fig. 4). Despite a broad spectrum of possible waves, most energy is transported in the synoptic scale by eddies at wavelengths between 2,000 and 8,000 km, demonstrating the dominant role of synoptic waves for the mid-latitudinal energy transport (Fig. S6). This is different from previous studies that find that transient eddies are responsible for the majority of mid-latitudinal energy transport (e.g. Peixoto and Oort, 1992), since planetary waves may also be transient. The peak transport of synoptic waves is at around 45° latitude, the location of the climatological storm tracks (Priestley and Catto, 2022) (Hoskins and Hodges, 2002, 2005), and coincides with the zone of largest total energy transport. Hence, synoptic waves advect energy from the subtropics (< 40°) to the extra-tropics (Fig. 5d).

Extra-tropical synoptic waves transport approximately two thirds of their energy in dry form and one third in latent form, with the latent contribution being a bit slightly more important in the low mid-latitudes and less important in the polar regions (Fig. 5b,c). Synoptic Despite transporting more dry than moist energy, synoptic eddies are responsible for the majority of the extra-tropical moisture transport. Especially in the polar regions almost all moisture transport is by synoptic waves, whereas dry transport in the polar regions occurs at both synoptic and planetary scales.

### Planetary transport

The planetary energy transport is almost similar in both hemispheres, different from the quasi-stationary transport that which is mainly relevant in the NH (Fig. 1a, 4, 5a). The planetary transport is similar in the subtropics and low mid-latitudes and only approximately 20% weaker in the higher mid-latitudes of the SH than the NH. This is in contrast to the previous interpretation that planetary transport being represented by the latter is in agreement with Trenberth and Stepaniak (2003a) underscoring that quasi-stationary transport is a primary factor in the extratropical NH. The latter study associates this quasi-stationary component is mainly relevant in the NH (e.g. Trenberth and Stepaniak, 2003a). This is the case since transport to the planetary scale, albeit without proof – a hypothesis which is confirmed by this study (Fig. 4). A new finding, that could partly be inferred from Fig. S3 of Lembo et al. (2019), is the near-symmetric structure of the planetary energy transport in both hemispheres. This symmetry could not have been anticipated by considering only quasi-stationary transport, since the planetary transport in the SH is mainly of transient character (Fig. 4), in agreement with Mo (1986).

In both hemispheres, the planetary transport has a highly relevant transient component in the SH (is similar in the subtropics and lower mid-latitudes. In the higher mid-latitudes and polar region of the SH it is approximately 20% weaker than in the

corresponding NH regions. Hence, eddies at similar spatial scales are transporting the energy in both hemispheres (see also Fig. 4)2), which is likely due to similar physical mechanisms in both hemispheres forming the energy-transporting eddies.

Generally two patterns of planetary transport are identified: 1) In the sub-tropics, most planetary transport is associated with quasi-stationary moisture transport,  $\widetilde{vQ}_{plan}^{q-s}$ . These waves represent subtropic presumably represent subtropical high-pressure and monsoon systems, which can prevail for several weeks. The planetary moisture transport leads to humidity divergence in the tropics and convergences in the sub- and extra-tropics (Fig. 5e).

2) In the extra-tropics, planetary eddies mainly transport dry static dry energy and only little moisture. In the polar regions, this planetary energy transport is almost as important as synoptic transport. The peak in energy transport by planetary waves,  $\widetilde{vE}_{plan}$ , is at the polar boundary around 60° latitude in both hemispheres (Fig. 5a,c), hence further poleward to than the peak in synoptic transport. Hence the planetary dry static at 45°. Thus, the planetary dry transport,  $\widetilde{vD}_{plan}$ , leads to energy divergence in the sub-tropics and mid-latitudes and convergence in the polar regions (Fig. 5f). The most remarkable difference between the hemispheres is that These planetary waves are transient in the extra-tropical mainly transient (Fig. 4: 70%) in the mid-latitudinal SH, whereas often the quasi-stationary in its northern counterpart component dominates (60%) in the corresponding NH region, which agrees with Peixoto and Oort (1992). However, in the high latitudes of the SH, a considerable fraction of the planetary transport is quasi-stationary.

### Meridional overturning circulation

The meridional overturning circulation,  $\widetilde{vE}_{meri}$ , and its role in transporting energy poleward have long been known (e.g. Hadley, 1735; Lorenz, 1967; Peixoto and Oort, 1992). It constitutes the The Hadley circulation in the tropics, which is dominating dominates the energy transport in that region. The annual-mean total energy transport,  $\widetilde{vE}_{meri}$ , by the Hadley circulation is small compared to the latent,  $\widetilde{vQ}_{meri}$ , and dry static components,  $\widetilde{vD}_{meri}$ , due to compensation between these two components thermally-direct dry component,  $\widetilde{vD}_{meri}$ , and to the thermally-indirect latent component,  $\widetilde{vQ}_{meri}$ , since the latter largely compensates the former (Fig. 5), and due to a compensation between the summer and winter season (see section a-c). Further, the annual-mean transport by the Hadley circulation is small, since transport into the tropical winter hemisphere originates from the equatorial summer hemisphere, whereby the transport partly compensates (see Section 4.2).

The

In the mid-latitudes, the meridional circulation,  $\widetilde{vE}_{meri}$ , features the thermally-indirect Ferrel cell in the mid-latitudes with a peak around 53°, which is almost twice as strong in the SH than NH. The transport by the Ferrel cell is mainly in form of dry static the form of dry energy which is to a small amount extent compensated by moisture transport being thermally direct. In the NH, the Ferrel cell eddy-driven Ferrel cell (Vallis, 2017), spans the whole extra-tropics including the Arctic. In the SH, a thermally-direct polar cell is evident in the dry static dry transport,  $\widetilde{vD}_{meri}$ , which is primarily driven by katabatic flow from Antarctica as noted by Trenberth and Stepaniak (2003a). Different to previous studies by for example Peixoto and Oort (1992) a NH polar cell is not evident in the here-utilised ERA-5 dataset, neither in the annual-mean nor in the summer or winter season (Sec. 4.2). In the Arctic, energy is transported by synoptic and planetary eddies favouring the formation of a Ferrel cell,

470 whereas zonal symmetric katabatic flows, as observed in the Antarctic, do not develop due to the lack of a large ice dome centred over the pole.

## Mesoscale transport

In contrast to synoptic and planetary waves, mesoscale waves,  $\tilde{vE}_{meso}$ , at scales smaller than 2,000 km, are only responsible for a negligible part of the energy and moisture transport at all latitudes (Fig. 2, S6), well in accordance with Graversen and Burtu (2016), who show that wavenumbers 0-10 are responsible for almost all the majority of the energy transport at 475 all latitudes. Atmospheric models may have larger challenges to reproduce mesoscale eddies as compared to eddies at larger scales. However, ERA5 at a horizontal grid spacing of  $\approx 30$  km is able to reproduce mesoscale cyclones, such as polar lows (Stoll et al., 2021), and hence the negligible importance of mesoscale eddies for the total energy transport appears reasonable. Due to its negligible role, we include the mesoscale into the synoptic transport for the remainder of this study, such that the sum of all scale components yields the total transport.

## 480 4.2 Seasonal transport

Some transport patterns become more apparent when seasons are considered analysed separately. The NH summer and the SH winter are here defined by the months June to August, and the NH winter and the SH summer by the months December to February. In spring and autumn the energy transport is mainly similar to the annual-mean transport (Fig. 5, S7).

485 Due to seasonal variations in the thermal contrast between the equator and poles, more energy is transported poleward in the winter than in the summer hemisphere (Fig. 6a,d) in good agreement with previous studies (e.g. Peixoto and Oort, 1992). The seasonality in the transport is larger in the NH than the SH, as also noted by Trenberth and Stepaniak (2003a). This is effected by a larger annual cycle in the temperature cycle in the NH due to its large continents having a smaller heat capacity than the oceans in the SH. Still, the two hemispheres share many characteristics in the atmospheric energy transport when it comes to seasonality. In spring and autumn the energy transport is in the main features similar to the annual-mean 490 transport (Fig. 5, S7).

The zone location separating northward and southward total transport is the energy flux equator (Adam et al., 2016), is at around 10° latitude in the summer hemisphere (Fig. 6d), the location of the intertropical convergence zone (ITCZ). This is close to the ascending branch of the Hadley circulation (Vallis, 2017, p.514). In the tropics, the meridional overturning circulation,  $\tilde{vE}_{meri}$ , is most important (Fig. 6, blue). It transports energy from around ITCZ the summer tropics to the winter subtropics, whereas moisture,  $\tilde{vQ}_{meri}$ , is advected in the opposite direction.

495 In contrast to the planetary transport,  $\tilde{vE}_{plan}$  the extra-tropics of both hemispheres, the synoptic transport,  $\tilde{vE}_{syno}$ , is little influenced by seasonality, in broad agreement with results from wavenumber separated transport of the NH mid-latitudes in Lembo et al. (2019) and with transient transport in Trenberth and Stepaniak (2003a). In the extra-tropics of both hemispheres contrast, the planetary transport,  $\tilde{vE}_{plan}$ , has a strong seasonality, being highly relevant in winter, but almost absent in summer. Hence, 500 the summer is dominated by synoptic transport,  $\tilde{vE}_{syno}$ . Differently, in winter both planetary and synoptic waves are highly relevant for the energy transport. In the NH winter, planetary waves,  $\tilde{vE}_{plan}$ , contribute to more transport than do synoptic

waves, mainly by ~~its~~their quasi-stationary component,  $\widetilde{vE}_{plan}^{q-s}$ . In the SH winter, planetary transport is also important, but mostly in ~~a~~its transient form,  $\widetilde{vE}_{plan}^{tran}$ , whereas its stationary part is small as noted previously (Oort and Peixoto, 1983).

In the subtropics of the summer hemisphere, quasi-stationary planetary waves,  $\widetilde{vE}_{plan}^{q-s}$ , are among the largest ~~contributor~~  
505 contributors to poleward energy transport (Fig. 6d). These waves are transporting energy mainly in the form of moisture,  $\widetilde{vQ}_{plan}^{q-s}$  (Fig. 6e) ~~and appear to represent, presumably reflecting~~ the summer monsoon and long-lasting sub-tropical high-pressure systems.

### 4.3 Inter-annual variability

In this study, the inter-annual variability in the energy transport is computed by the standard deviation of the annual-mean  
510 transport. The total energy transport,  $\widetilde{vE}$ , is only varying by a few percent between years for all latitudes (Fig. 7a). However, the inter-annual variability in the individual components is up to three times larger than the variability in the total transport especially in the extra-tropics (Fig. 7a). Hence, large transport in one component is typically compensated by smaller transport in another component, as also noted by Trenberth and Stepaniak (2003a) and Lembo et al. (2019).

In contrast to the total energy transport, the variability of the moisture transport components ~~total moisture transport,  $\widetilde{vQ}$ , are~~  
515 ~~rather summing up to the total variance is larger than the variability of its individual scale components (Fig. 7b). Hence, the~~  
~~moisture transport components are not compensating each other in the same manner as the total energy transport components.~~  
~~Instead, the compensation of the components of the total energy transport is in form of dry energy (Fig. 7b)-c).~~

We hypothesise that the different co-variability of the scale contributions for the total energy and moisture transport are due to ~~different mechanisms leading to energy and moisture transport as further explained in a subsequent study~~their different  
520 underlying mechanisms. Preliminary results point towards the annual-mean energy transport being induced by the meridional temperature, i.e. energy gradient in the manner of a diffusion process with a globally almost constant diffusion coefficient. Hence, large transport in one component reduces the temperature gradient, leading to less transport in another component. Differently, moisture is a tracer of the atmospheric circulation and therefore not described by a diffusion process, such that the components do not compensate in a similar manner as for the total energy transport.

525 The tropics feature large inter-annual variability in the moisture transport,  $\widetilde{vQ}$ , and approximately equally large variability in the ~~dry static~~dry transport,  $\widetilde{vD}$ , ~~whereas~~ (Fig. 7b,c). ~~The large total variability in the moist and dry energy transports is almost entirely due to variability in the meridional components, which is not surprising since the meridional components are responsible for most of the moist and dry energy transport in the tropics (Fig. 5b,c, 6b,c,e,f).~~ However, the variability in total transport,  $\widetilde{vE}$ , is only a fifth of the moisture transport variability (Fig. 7). ~~This means that in the tropics, anomalous latent transport is typically compensated by opposed anomalies in the dry static transport~~a,b. Hence, ~~the~~ the Hadley circulation transports more latent energy in some years, although this has little effect on if a strong Hadley circulation in one year is effecting a larger than usual thermally direct dry energy transport, it will likely also effect a larger than usual thermally indirect latent energy transport, such that the total energy ~~transport~~transported is more or less constant between years.

530

535 In the extra-tropics, the planetary transport,  $\widetilde{vE}_{plan}$ , ~~exhibits~~ is the component exhibiting the largest inter-annual variability and varies by approximately 10% (Fig. 7), even though a. This is remarkable since the annual-mean planetary transport is

mainly smaller (Fig. 5) than the synoptic transport,  $\widetilde{vE}_{syno}$ , which varies by . Consequentially, the planetary transport,  $\widetilde{vE}_{plan}$ , varies from year to year by approximately 10% in the mid-latitudes and 15–20% in the polar regions, whereas the synoptic transport,  $\widetilde{vE}_{syno}$  varies only around 5%. The large planetary variability is mainly attributed to its quasi-stationary component,  $\widetilde{vE}_{plan}^{q-s}$ , whereas its transient component,  $\widetilde{vE}_{plan}^{tran}$ , is much less variable (not shown). This demonstrates the "quasiness" of the quasi-stationary transport, which is being the transport component varying that varies most from year to year. This appears to express the importance of annual modes creating presumably reflects the role of (inter-)annual modes of climate variability in favouring different quasi-stationary planetary transport and changing states between circulations and planetary transports in different years.

The extra-tropical moisture transport,  $\widetilde{vQ}$ , is varying approximately equally for planetary,  $\widetilde{vQ}_{plan}$ , and synoptic waves,  $\widetilde{vQ}_{syno}$  (Fig. 7b). However, due to synoptic waves being responsible for most of the moisture transport in the extra-tropics (Fig. 5b), the variability fraction is considerably higher for the planetary than the synoptic moisture transport.

## 5 Discussion and conclusion

In this study, we analyse the global atmospheric circulation by separating the meridional energy transport of the years 1979–2021 in the ERA5 reanalysis by spatial scales, by moisture and dry static moist and dry components, and by quasi-stationary and transient parts. We For separating the energy transport by scales for all latitudes, we apply a new approach by using the wavelength instead of the wavenumber for separating the energy transport by scales for all latitudes. We argue utilised previously (e.g. Graversen and Burtu, 2016).

We demonstrate that a separation between planetary and synoptic transport by synoptic and planetary eddies at a wavelength of 8,000 km reflects the physically-grounded distinction between baroclinically-induced and other eddies. Moreover, we show that the separation wavelength of 8000 km and towards mesoscale eddies at 2,000 is largely latitude-independent. This separation wavelength approximately agrees with the traditional separation between transient and quasi-stationary eddies, as most eddy transport smaller than 8000 km is of transient character, whereas most quasi-stationary transport occurs at the planetary scale larger than 8000 km. Despite the latter, considerable planetary energy transport is of transient character, especially in the extratropical SH.

It should be noted that the scale separation is implemented in a continuous manner such the largest eddy with a wavelength smaller than 8000 km capture our intuitive understanding of these waves as well as previously demonstrated differences between the scales is partitioned between the planetary and synoptic scale. This implies that the planetary transport includes waves of size around 8000 km, whereas synoptic transport is by waves strictly smaller than 8000 km.

Synoptic eddies with a wavelength of almost 8000 km may appear large scale. However, most baroclinically-induced and most transient energy transport organises at wavelengths around 5000 km at all latitudes (Fig. 2, 3), well in agreement with the predicted length by dry-baroclinic theory (Vallis, 2017). Despite the maximum around 5000 km, the baroclinically-induced and transient energy transport occurs in a wavelength band between approximately 2000 and 8000 km, hence separating at around 5000 km would be misleading. It should further be noted that one synoptic wave includes both a low and a high pressure system.

570 Hence, a 2000– 8000 km range implies that synoptic cyclones and anticyclones feature a typical diameter of between 1000 and smaller than 4000 km, or that the typical distance between the cores of two independent (anti)cyclones is between 2000 and 8000 km. This appears reasonable from comparison with weather maps. Even in situations of cyclone clusters, arguably situations where the distance between cyclones is unusually low, the spacing between cyclonic centres is around 2000 km (e.g. Weijenborg and Spengler, 2020, Fig. 2d-f), the lower end of the here-defined synoptic scale. Note, that the cyclones of that cluster share a common front, hence appear not independent. The distance of the cyclones is in north-eastward direction, 575 whereas the next cyclones in the zonal direction are at larger distances of around 5000 km. Hence, our methodology relying on a zonal Fourier decomposition appears to be accurate for such situations.

580 A ~~clear single, sharp~~ spatial separation between the synoptic and planetary ~~scale-scales~~ may not exist ~~in the real world~~, but a spatial decomposition has been demonstrated to be useful for better understanding the atmospheric circulation and its impact on ~~the local~~ ~~regional~~ climate (Baggett and Lee, 2015; Graversen and Burtu, 2016; Röhlisberger et al., 2019). Here, we provide further arguments for the usefulness of ~~the~~ separating the energy transport by ~~the~~ spatial scale.

585 Different from the classical separation into quasi-stationary and transient energy transport, the ~~transport is spatial scales of the transport are~~ quite similar in ~~the spatial scales for~~ both hemispheres, pointing towards ~~the scale separation being a rather general method. This is most obvious in the quasi-stationary transport,  $\tilde{vE}_{plan}^{q-s}$ , which is~~ similarities in the contribution of active physical mechanisms. The most pronounced difference between the two separation methods is that planetary transport,  $\tilde{vE}_{plan}$ , is broadly similar in both hemispheres, whereas quasi-stationary transport,  $\tilde{vE}^{q-s}$ , is mainly important in the NH extra-tropical winter, whereas planetary transport is highly relevant in both hemispheres.

590 In the annual-mean, most energy and moisture in the extra-tropics is transported by synoptic eddies,  $\tilde{vE}_{syno}$ . It is ~~astonishing that despite all possible eddies, waves~~ ~~remarkable that in the large range of atmospheric eddies, those~~ at scales in the ~~rather narrow band between 2,000 and 8,000~~ band between 2000 and 8000 km are responsible for the majority of the meridional energy transport for the whole extra-tropics. ~~As baroclinic eddies lay within this band, this~~ This points towards the importance of baroclinic instability for inducing the extra-tropical energy transport as ~~long being suspected has long been hypothesised~~ (Holton and Hakim, 2013). However, other ~~mechanism mechanisms~~ may contribute to the formation of eddies in ~~this band the synoptic scale~~. Hence, a future study is planned to investigate causes and effects of energy transport at different scales.

595 The synoptic energy transport reveals to be little influenced by the season. In contrast, extra-tropical planetary transport,  $\tilde{vE}_{plan}$  is of major importance ~~in winter only in the winter season~~ mainly by transporting ~~dry static dry~~ energy,  $\tilde{vD}_{plan}$ , ~~but less relevant in summer~~. In winter around the Arctic boundary, quasi-stationary planetary waves,  $\tilde{vE}_{plan}^{q-s}$ , ~~are dominating~~ dominate the energy transport. Such quasi-stationary planetary waves around the polar boundaries of both hemispheres feature the transport component with globally the largest inter-annual variability.

600 Also known characteristics of the atmospheric circulation are reproduced in this study, such as the dominance of the Hadley circulation in the tropics for transporting ~~of~~ energy,  $\tilde{vE}_{meri}$ , to the winter hemisphere, and transporting ~~of~~ moisture,  $\tilde{vQ}_{meri}$ , in the opposite direction. In the subtropical summer, quasi-stationary planetary waves transporting moisture,  $\tilde{vQ}_{plan}^{q-s}$ , are the largest contributor to poleward energy transport, which is associated with monsoon systems.

In this study, the atmospheric transport is analysed on an annual-mean and seasonal-mean basis, whereas ~~individual weather events feature a large variety of transport patterns (Lembo et al., 2019)~~ on shorter timescales the transport can be highly sporadic and displays large deviations from climatology (Swanson and Pierrehumbert, 1997; Messori and Czaja, 2013; Lembo et al., 2019). Some planetary transport events in the extra-tropics are for example equatorward. Hence, when the seasonal-mean ~~poleward~~ planetary transport is close to zero, ~~it means this can either mean that the planetary transport is generally small or~~ that poleward and equatorward transport events are balancing each other. The intra-seasonal distribution of the different transport components ~~is will be~~ investigated in a follow-up study. ~~Further, a follow-up study investigates how the energy transport in its components may change with global warming. Another option for investigating the spatio-temporal scale of eddies is the usage of Hayashi spectra as in Dell'Aquila et al. (2005) that performs a Fourier decomposition in both space and time.~~

*Data availability.* The ERA-5 dataset is publicly available. The computed decomposition of the energy transport based on ERA-5 and the code for the analysis is willingly provided on request.

*Competing interests.* The authors declare no competing interests.

*615 Acknowledgements.* Thanks to ECMWF for providing access to data from the ERA5 reanalysis. The data were partly processed at the supercomputer FRAM and stored at NIRD, both provided by the Norwegian Research Infrastructure Services (NRIS) Sigma2 AS under the projects NN9348K and NS9063K, respectively.

## References

Adam, O., Bischoff, T., and Schneider, T.: Seasonal and Interannual Variations of the Energy Flux Equator and ITCZ. Part I: Zonally  
620 Averaged ITCZ Position, *Journal of Climate*, 29, 3219 – 3230, <https://doi.org/10.1175/JCLI-D-15-0512.1>, <https://journals.ametsoc.org/view/journals/clim/29/9/jcli-d-15-0512.1.xml>, 2016.

Ali, S. M., Martius, O., and Röhlisberger, M.: Recurrent Rossby wave packets modulate the persistence of dry and wet spells across the globe, *Geophys. Res. Lett.*, 48, e2020GL091452, 2021.

Baggett, C. and Lee, S.: Arctic warming induced by tropically forced tapping of available potential energy and the role of the planetary-scale  
625 waves, *Journal of the Atmospheric Sciences*, 72, 1562–1568, 2015.

Bjerknes, J.: On the structure of moving cyclones, *Geophys. Publ.*, 1, 8 pp, 1919.

Businger, S. and Reed, R. J.: Cyclogenesis in cold air masses, *Weather and Forecasting*, 4, 133–156, 1989.

Dell'Aquila, A., Lucarini, V., Ruti, P. M., and Calmanti, S.: Hayashi spectra of the northern hemisphere mid-latitude atmospheric variability  
in the NCEP–NCAR and ECMWF reanalyses, *Climate Dynamics*, 25, 639–652, 2005.

630 Graversen, R. G.: Do changes in the midlatitude circulation have any impact on the Arctic surface air temperature trend?, *Journal of climate*, 19, 5422–5438, 2006.

Graversen, R. G. and Burtu, M.: Arctic amplification enhanced by latent energy transport of atmospheric planetary waves, *Quarterly Journal  
of the Royal Meteorological Society*, 142, 2046–2054, 2016.

Graversen, R. G., Stoll, P. J., and Rydsaa, J. H.: Hvorfor er Arktis det området i verden med raskest oppvarming?, *Naturen*, 145, 160–167,  
635 2021.

Hadley, G.: VI. Concerning the cause of the general trade-winds, *Philosophical Transactions of the Royal Society of London*, 39, 58–62,  
1735.

Heiskanen, T., Graversen, R. G., Rydsaa, J. H., and Isachsen, P. E.: Comparing wavelet and Fourier perspectives on the decomposition  
of meridional energy transport into synoptic and planetary components, *Quarterly Journal of the Royal Meteorological Society*, 146,  
640 2717–2730, 2020.

Hersbach, H., Bell, B., Berrisford, P., Hirahara, S., Horányi, A., Muñoz-Sabater, J., Nicolas, J., Peubey, C., Radu, R., Schepers, D., et al.:  
The ERA5 global reanalysis, *Quarterly Journal of the Royal Meteorological Society*, 146, 1999–2049, 2020.

Hofsteenge, M. G., Graversen, R. G., Rydsaa, J. H., and Rey, Z.: The impact of atmospheric Rossby waves and cyclones on the Arctic sea  
ice variability, *Climate Dynamics*, <https://doi.org/doi.org/10.1007/s00382-022-06145-z>, 2022.

645 Holton, J. and Hakim, G.: An Introduction to Dynamic Meteorology, vol. 5, Academic Press, New York, USA, 2013.

Hoskins, B. J. and Hodges, K. I.: New perspectives on the Northern Hemisphere winter storm tracks, *Journal of the Atmospheric Sciences*,  
59, 1041–1061, 2002.

Hoskins, B. J. and Hodges, K. I.: A new perspective on Southern Hemisphere storm tracks, *Journal of Climate*, 18, 4108–4129, 2005.

Lee, S., Woods, C., and Caballero, R.: Relation between Arctic moisture flux and tropical temperature biases in CMIP5 simulations and its  
650 fingerprint in RCP8.5 projections, *Geophysical Research Letters*, 46, 1088–1096, 2019.

Lembo, V., Messori, G., Graversen, R., and Lucarini, V.: Spectral Decomposition and Extremes of Atmospheric Meridional Energy Transport in the Northern Hemisphere Midlatitudes, *Geophysical Research Letters*, 46, 7602–7613,  
<https://doi.org/https://doi.org/10.1029/2019GL082105>, 2019.

Lorenz, E.: The nature and theory of the general circulation of the atmosphere, *World meteorological organization*, 161, 1967.

655 Markowski, P. and Richardson, Y.: Mesoscale meteorology in midlatitudes, vol. 2, John Wiley & Sons, Chichester, UK, <https://doi.org/https://doi.org/10.1002/9780470682104>, 2011.

660 Messori, G. and Czaja, A.: On the sporadic nature of meridional heat transport by transient eddies, *Quarterly Journal of the Royal Meteorological Society*, 139, 999–1008, 2013.

665 Mo, K. C.: Quasi-Stationary States in the Southern Hemisphere, *Monthly Weather Review*, 114, 808 – 823, [https://doi.org/10.1175/1520-0493\(1986\)114<0808:QSSITS>2.0.CO;2](https://doi.org/10.1175/1520-0493(1986)114<0808:QSSITS>2.0.CO;2), 1986.

670 Oort, A. H. and Peixoto, J. P.: Global angular momentum and energy balance requirements from observations, in: *Advances in Geophysics*, vol. 25, pp. 355–490, Elsevier, 1983.

675 Orlanski, I.: A rational subdivision of scales for atmospheric processes, *Bulletin of the American Meteorological Society*, pp. 527–530, 1975.

680 Papritz, L. and Dunn-Sigouin, E.: What configuration of the atmospheric circulation drives extreme net and total moisture transport into the Arctic, *Geophysical Research Letters*, 47, e2020GL089769, 2020.

685 Peixoto, J. P. and Oort, A. H.: *Physics of climate*, American Institute of Physics, 1992.

Priestley, M. D. K. and Catto, J. L.: Future changes in the extratropical storm tracks and cyclone intensity, wind speed, and structure, *Weather and Climate Dynamics*, 3, 337–360, <https://doi.org/10.5194/wcd-3-337-2022>, 2022.

690 Rossby, C.-G.: Relation between variations in the intensity of the zonal circulation of the atmosphere and the displacements of the semi-permanent centers of action, *J. mar. Res.*, 2, 38–55, 1939.

Röthlisberger, M., Frossard, L., Bosart, L. F., Keyser, D., and Martius, O.: Recurrent synoptic-scale Rossby wave patterns and their effect on the persistence of cold and hot spells, *Journal of Climate*, 32, 3207–3226, 2019.

700 Rydsaa, J. H., Graversen, R., Heiskanen, T. I. H., and Stoll, P.: Changes in atmospheric latent energy transport into the Arctic: Planetary versus synoptic scales, *Quart. J. Roy. Meteorol. Soc.*, 2021.

705 Shaw, T., Baldwin, M., Barnes, E. A., Caballero, R., Garfinkel, C., Hwang, Y.-T., Li, C., O'gorman, P., Rivière, G., Simpson, I., et al.: Storm track processes and the opposing influences of climate change, *Nature Geoscience*, 9, 656–664, 2016.

710 Stoll, P. J., Spengler, T., Terpstra, A., and Graversen, R. G.: Polar lows – moist-baroclinic cyclones developing in four different vertical wind shear environments, *Weather and Climate Dynamics*, 2, 19–36, <https://doi.org/10.5194/wcd-2-19-2021>, 2021.

715 Swanson, K. L. and Pierrehumbert, R. T.: Lower-tropospheric heat transport in the Pacific storm track, *Journal of the atmospheric sciences*, 54, 1533–1543, 1997.

720 Trenberth, K. E.: Climate diagnostics from global analyses: Conservation of mass in ECMWF analyses, *Journal of Climate*, 4, 707–722, 1991.

725 Trenberth, K. E. and Caron, J. M.: Estimates of meridional atmosphere and ocean heat transports, *Journal of Climate*, 14, 3433–3443, 2001.

730 Trenberth, K. E. and Stepaniak, D. P.: Covariability of components of poleward atmospheric energy transports on seasonal and interannual timescales, *Journal of climate*, 16, 3691–3705, 2003a.

735 Trenberth, K. E. and Stepaniak, D. P.: Seamless poleward atmospheric energy transports and implications for the Hadley circulation, *Journal of Climate*, 16, 3706–3722, 2003b.

740 Vallis, G. K.: *Atmospheric and oceanic fluid dynamics*, Cambridge University Press, 2017.

745 Vihma, T., Graversen, R., Chen, L., Handorf, D., Skific, N., Francis, J. A., Tyrrell, N., Hall, R., Hanna, E., Uotila, P., et al.: Effects of the tropospheric large-scale circulation on European winter temperatures during the period of amplified Arctic warming, *Int. J. Climatol.*, 40, 509–529, 2020.

Weijenborg, C. and Spengler, T.: Diabatic heating as a pathway for cyclone clustering encompassing the extreme storm Dagmar, *Geophysical Research Letters*, 47, e2019GL085 777, 2020.

Wirth, V., Riemer, M., Chang, E. K., and Martius, O.: Rossby wave packets on the midlatitude waveguide—A review, *Monthly Weather Review*, 146, 1965–2001, 2018.

695 Wolf, G. and Wirth, V.: Diagnosing the Horizontal Propagation of Rossby Wave Packets along the Midlatitude Waveguide, *Monthly Weather Review*, 145, 3247 – 3264, <https://doi.org/10.1175/MWR-D-16-0355.1>, 2017.

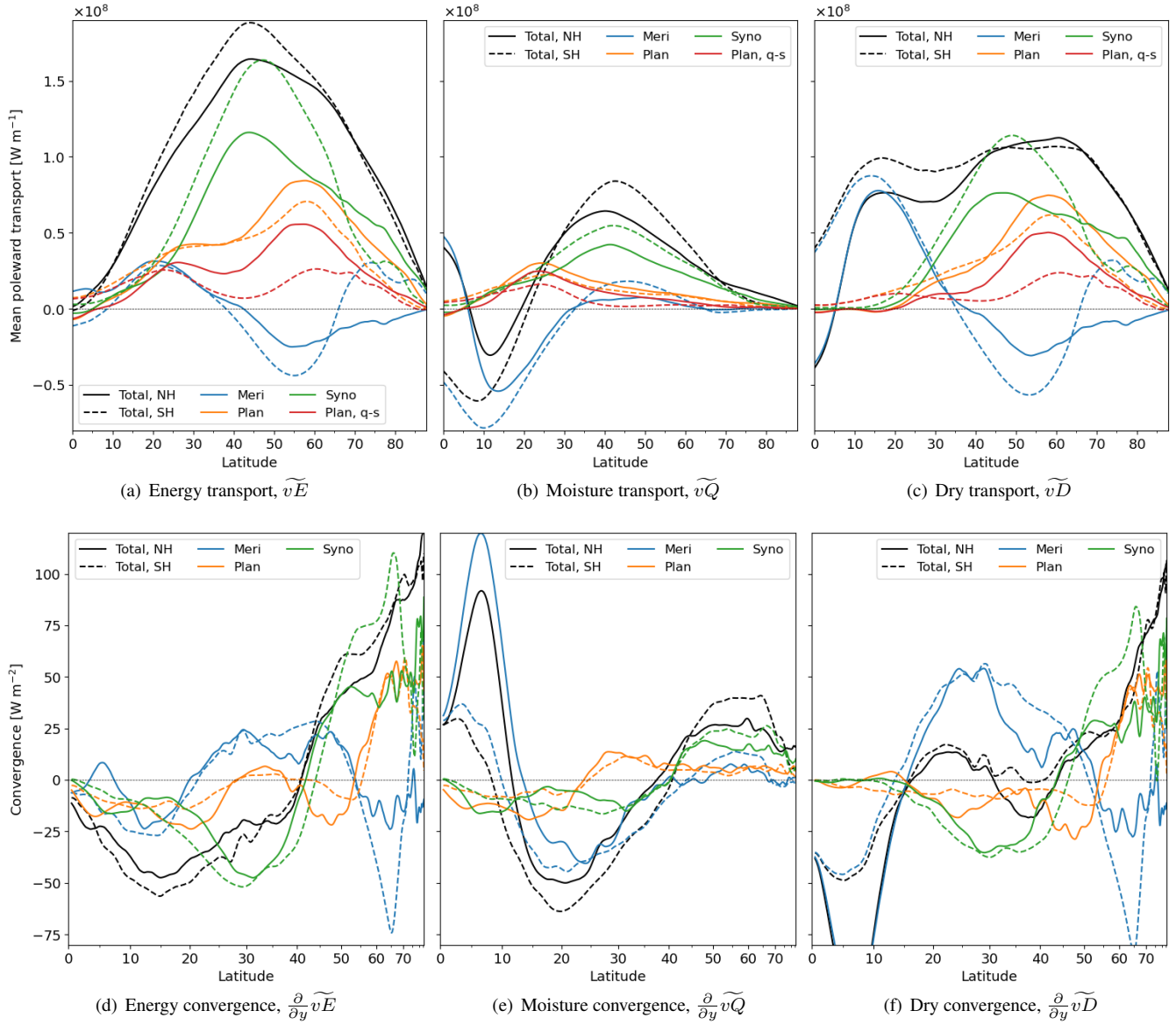


**Figure 5.** (a) Annual-mean, zonal-mean poleward atmospheric energy transport from ERA5 for the years 1979–2021. The transport of the Northern and Southern Hemisphere are depicted in solid and dashed lines, respectively. The total energy transport (black) is divided into the zonally symmetric meridional overturning circulation (blue) and wave components at the planetary (orange, waves  $> 8,000$  km) and synoptic scales (green,  $< 8,000$  km). The quasi-stationary contribution of the planetary transport on a monthly scale is depicted in red. (b) and (c) as (a) but for the latent and dry static energy transport components, respectively. (d)–(f) Resulting convergence of atmospheric energy from the transport components presented in (a)–(c), with exception of but for simplicity omitting the convergence of quasi-stationary planetary transport. The latitudes on the x-axis are scaled to represent equal surface areas, such that the integrated convergence in each component becomes zero.

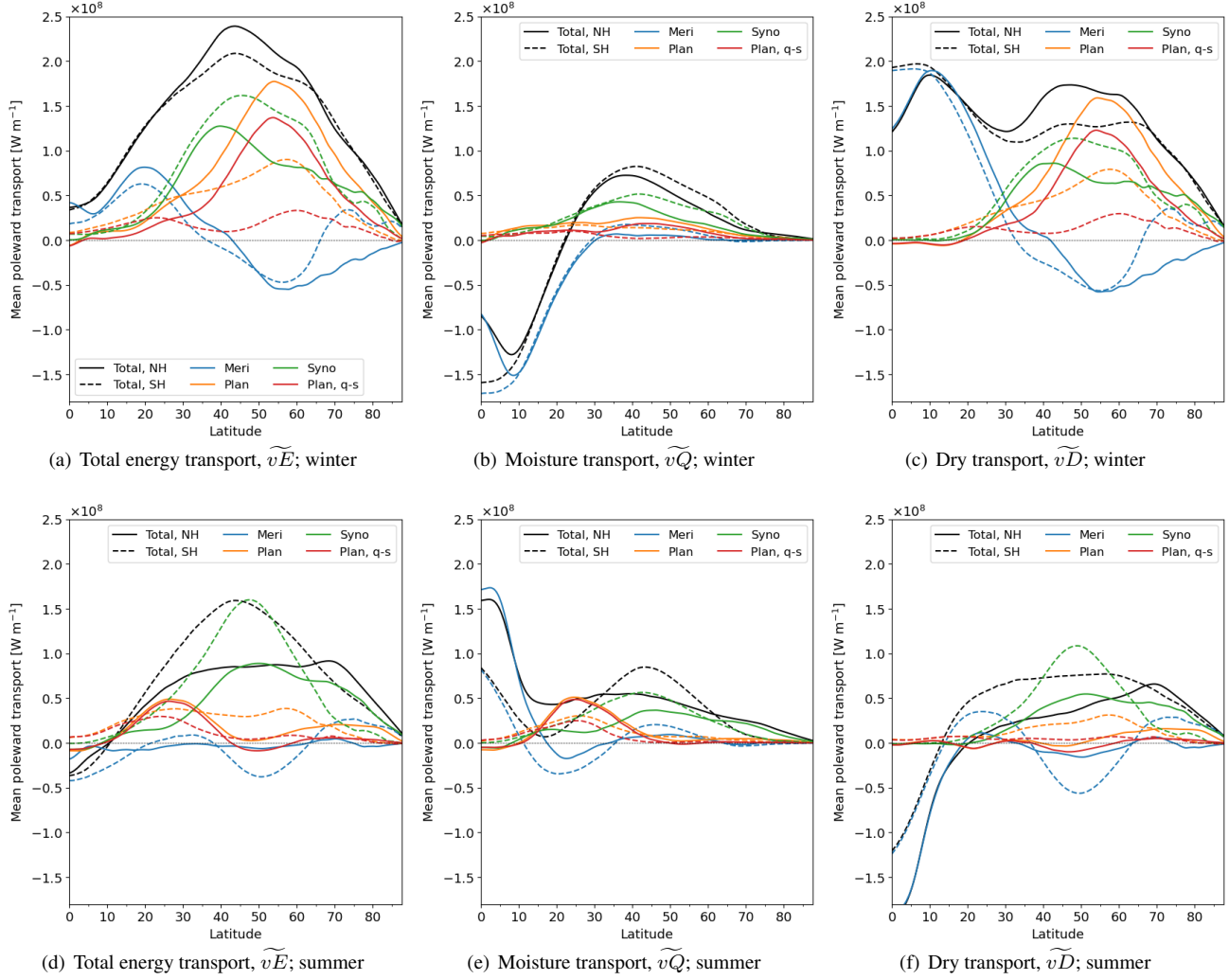


**Figure 6.** As Figure 5a-c, but for the seasonal-mean transport of (a-c) winter, and (d-f) summer for (a,d) the total energy transport, (b,e) its latent component, and (c,f) its **dry-static-dry** component.

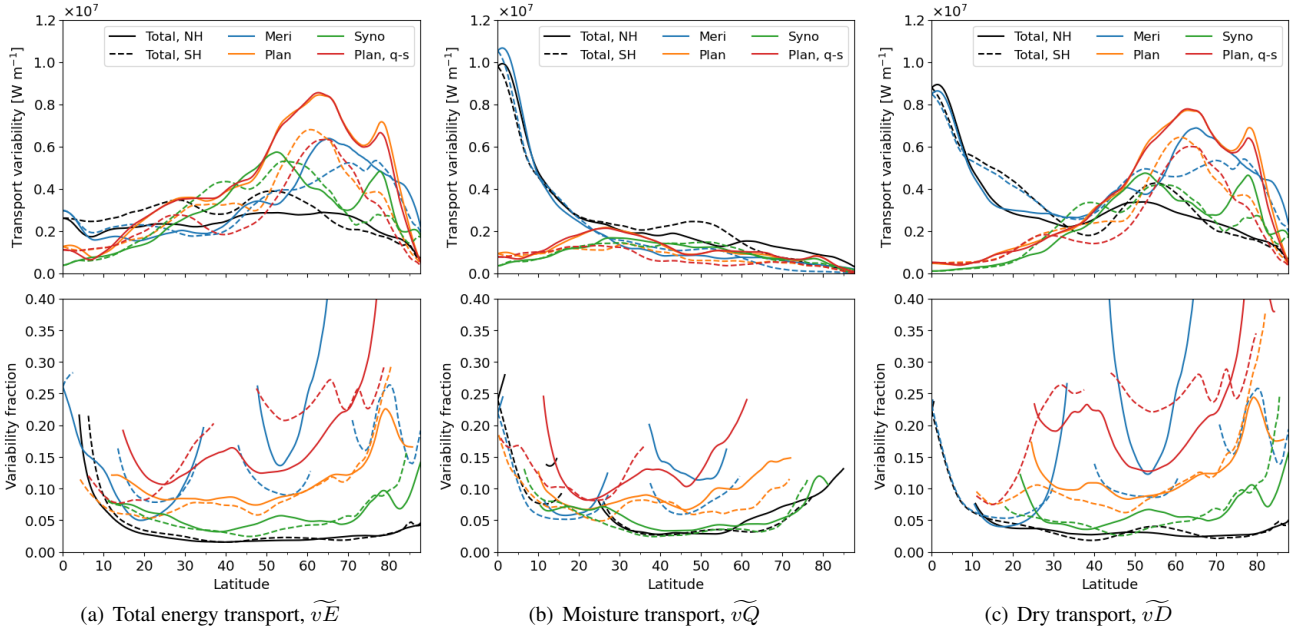


**Figure 7.** (a, upper panel) Inter-annual variability in the meridional energy transport, computed as the standard deviation in the annual transport, from ERA5 for the years 1979 – 2021 (black). The energy transport is divided into the meridional overturning circulation (blue) and wave components at the planetary (orange) and synoptic (green) scales. Solid and dashed lines depict the Northern and Southern Hemisphere, respectively. (Lower panel) The fraction of the variance of each transport component related to its absolute mean transport. Values are masked at latitudes  $\pm 5^\circ$  where the mean transport crosses zero [and/or](#) where the absolute mean is smaller than 5% of the zonal-maximum of the total transport. (b) and (c) as (a) but for the latent and [dry static](#) [dry](#) energy transport.